

Diffusion in a granular fluid. II. Simulation

James Lutsko

Center for Nonlinear Phenomena and Complex Systems, Université Libre de Bruxelles Campus Plaine, CP 231 1050 Bruxelles, Belgium

J. Javier Brey

Física Teórica, Universidad de Sevilla, Apartado de Correos 1065, E-41080 Sevilla, Spain

James W. Dufty

Department of Physics, University of Florida, Gainesville, Florida 32611

(Received 20 January 2002; published 17 May 2002)

The linear-response description for impurity diffusion in a granular fluid undergoing homogeneous cooling is developed in the preceding paper. The formally exact Einstein and Green-Kubo expressions for the self-diffusion coefficient are evaluated there from an approximation to the velocity autocorrelation function. These results are compared here to those from molecular-dynamics simulations over a wide range of density and inelasticity, for the particular case of self-diffusion. It is found that the approximate theory is in good agreement with simulation data up to moderate densities and degrees of inelasticity. At higher density, the effects of inelasticity are stronger, leading to a significant enhancement of the diffusion coefficient over its value for elastic collisions. Possible explanations associated with an unstable long wavelength shear mode are explored, including the effects of strong fluctuations and mode coupling.

DOI: 10.1103/PhysRevE.65.051304

PACS number(s): 45.70.Mg, 05.70.Ln

I. INTRODUCTION

Attempts to describe granular media in terms of a more fundamental underlying statistical mechanics have met with considerable success. As a prototype for this approach, in the preceding paper [1] standard linear-response methods from normal fluids have been applied, *mutatis mutandis*, to the case of an impurity particle diffusing in an isolated one component fluid of smooth inelastic hard spheres ($d=3$) or disks ($d=2$) of diameter σ . The collisions are characterized by a coefficient of normal restitution α . The isolated system (or with periodic boundary conditions), is not in the typical Gibbs state as for elastic collisions, but rather in a time-dependent homogeneous cooling state (HCS). It has been shown in [1], and will be elaborated further here, that this time-dependent HCS can be exactly transformed to a stationary-state description. In the present paper, this stationary-state description is evaluated by molecular-dynamics (MD) simulation to measure the mean-square displacement of the impurity, its velocity autocorrelation function, and the resulting diffusion coefficient defined in terms of a formal Einstein or Green-Kubo relation, respectively. For practical purposes, attention is restricted to the case of self diffusion, where the mechanical properties of the impurity are the same as those of the fluid particles.

The velocity autocorrelation function was approximated in [1] using a cumulant expansion and also by means of kinetic theory methods. In the usual first Sonine polynomial expansion for the latter, this leads to a simple exponential decay in an appropriate dimensionless time scale defined below. For the numerical results considered here, one further approximation is made in evaluating the decay rate, namely, two-particle velocity correlations are neglected. In this case, the results are the same as those obtained from the Enskog kinetic theory. Earlier studies of self diffusion [2] show ex-

cellent agreement of this theory with MD results at very low number density n , over a wide range of values for α . The present paper extends that study to higher densities. More specifically, three-dimensional systems with densities in the interval $0.1 \leq n^* \equiv n\sigma^3 \leq 0.75$, for $0.5 \leq \alpha \leq 1$, will be considered.

The HCS is known to be unstable under long wavelength perturbations or fluctuations [3]. To avoid this problem, the system size in most cases considered is chosen to be smaller than the critical wavelength. The latter is a function of the density and inelasticity, decreasing with increasing values of each. Consequently, at the highest densities and smallest α a small system of 108 particles is required. At moderate densities and inelasticities, a system size of 512 particles is used. The agreement of theory and simulation is found to be quite good for all α at $n^* \leq 0.25$ and for all densities at $\alpha \geq 0.9$. At higher densities and smaller α , significant discrepancies occur, with the diffusion coefficient obtained from MD being almost an order of magnitude greater than the theoretical estimate at $n^* = 0.75$ and $\alpha = 0.5$. The failure of the Enskog theory at high densities is well known for the case of elastic collisions, due to cage effects and correlated binary collisions. However, in that case the diffusion coefficient from MD is smaller than the theoretical prediction. Therefore, it is clear that a quite different density mechanism is effective for inelastic collisions.

It is reasonable to expect that the underlying instability is responsible in part for the above discrepancies. Although the instability is, in principle, avoided by the use of small systems, the latter is prone to large fluctuations. These are not quantitatively significant at $\alpha = 1$ but grow rapidly with decreasing α , as can be seen in the noise level for the kinetic temperature. This will be illustrated later on in Fig. 1. A related issue is the role of the instability in affecting the usual mode coupling corrections to the Enskog theory. Such

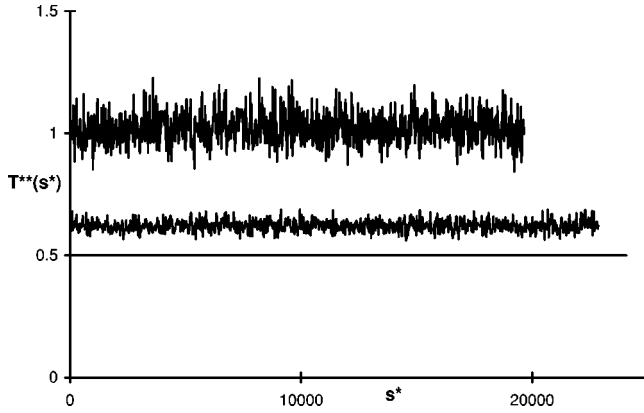


FIG. 1. Time evolution of the dimensionless steady temperature T^{**} as a function of scaled dimensionless time s^* for $n^*=0.5$. The lower curve is for $\alpha=1$, the middle for $\alpha=0.7$, and the upper for $\alpha=0.5$.

mode coupling terms arise from correlations of spontaneous fluctuations in the long wavelength hydrodynamic modes, which are significantly modified by the potential instability. Enhanced fluctuations will be addressed in the qualitative analysis of the data below.

The plan of the paper is as follows. In Sec. II, the relevant results in the preceding paper are shortly summarized, and a scale transformation, useful for practical purposes, is introduced. The equations of motion of the phase-space variables lead in a direct way to a steady-state simulation method for the HCS. Starting from an arbitrary initial condition, the system rapidly approaches a steady state, whose properties are simply related to those of the HCS. It is important to stress that this relationship is not approximate, but an *exact* consequence of a change of variables. In particular, the method to measure the mean-square displacement of a tagged particle as well as its velocity autocorrelation function is discussed in detail. Moreover, both quantities are shown to lead to equivalent results for the self-diffusion coefficients. Although in practice some discrepancies appear in the numerical results obtained by the two procedures, their origin is well understood.

Comparison of theory and simulation is also started in Sec. II, and completed in Sec. III. As mentioned above, the agreement is fairly good at low densities, but relevant effects, which are not taken into account by the theory developed in [1], show up even at moderate density. The peculiar nature of these effects for inelastic collisions is discussed. Numerical evidence is provided indicating that the underlying hydrodynamic instability associated with the shear mode plays an essential role in the “anomalous” behavior of the self-diffusion coefficient. Nevertheless, such changes in the diffusion constant do not compromise the existence of the diffusion process, which is confirmed for such conditions by simulation results for the mean-square displacement. Finally, Sec. IV contains a short summary of the results and also some indications of the possible extensions of the reported paper.

II. STEADY-STATE SIMULATION METHOD

To investigate the nature of diffusion in the HCS and to test the theoretical results presented in the preceding paper

[1], a more fundamental description via MD simulation will be considered. The HCS distribution function for a fluid of $N+1$ particles in d dimensions has the scaling form

$$\rho_{\text{HCS}}(\Gamma, t) = [\ell v(t)]^{-d(N+1)} \rho_{\text{HCS}}^*(\{\mathbf{q}_{ij}/\ell, \mathbf{v}_i/v(t)\}). \quad (1)$$

Here and in the following the notation is the same as in Ref. [1]. In particular, $v(t)$ is the thermal velocity defined in the usual way (with Boltzmann’s constant set equal to one) and $\ell = 1/n\sigma^{d-1}$ is proportional to the mean free path of the gas. The time dependence of the above distribution is due to collisional cooling and is determined from

$$\partial_t v(t) = -\frac{1}{2} \zeta(t) v(t), \quad (2)$$

where $\zeta(t)$ is the cooling rate. A direct simulation of the cooling fluid, as described by the Liouville dynamics in the actual phase variables, is difficult, since the rapid cooling of the fluid leads to numerical inaccuracies very soon. One method of dealing with this would be to periodically redefine the time scale of the simulation, so that the typical particle velocity remains of the order of unity. However, if the rescaling is only used to control the numerical stability of the simulation, the state being simulated would nevertheless be time dependent. For this reason, some simulation studies employ different type of thermostats, such as an externally imposed Brownian force or thermal boundaries, in order to generate a steady state. While these methods provide more or less realistic models of various experimental procedures, they obviously probe a state which is in some way related to, but not identical with, the homogeneous cooling state.

Soto and Mareschal [4], noting the fact that there is no intrinsic time scale in the dissipative hard-sphere model, have proposed to rescale all particle velocities after every collision, thus establishing a steady-state similar to that described in [1]. However, this procedure has the effect of replacing the binary collision dynamics of the dissipative hard-sphere model by an N -body dynamics, since the result of a collision is to alter *all* atomic velocities and not just those of the colliding atoms. It is reasonable to imagine that the binary dynamics is recovered in the infinite system limit, but the connection between the HCS and this dynamics is not clear for the case of the small systems considered in most of the MD simulations. Instead, we follow the procedure used in Ref. [5], according to which an *exact* mapping of the HCS onto a steady state is exploited as the basis of the simulation method. Following the ideas developed in [1], all velocities are scaled relative to $v(t)$ and the dimensionless time is given by

$$ds(t) = v(t) dt / \ell. \quad (3)$$

This time scale is a measure of the average collision number. The corresponding Liouville equation in these variables supports a stationary HCS solution given by $\rho_{\text{HCS}}^*(\{\mathbf{q}_{ij}^*, \mathbf{v}_i^*\})$, where $\mathbf{q}_i^* = \mathbf{q}_i / \ell$ and $\mathbf{v}_i^* = \mathbf{v}_i / v(t)$. Moreover, the average value of any phase function $A(\{\mathbf{q}, \mathbf{v}\})$ is given by Eq. (40) of Ref. [1].

$$\langle A; t \rangle = \int d\Gamma^* \rho^*(\Gamma^*) A(\{\mathcal{L}^* \mathbf{q}_i^*(s), v(t) \mathbf{v}_i^*(s)\}). \quad (4)$$

The dynamics in the phase space is obtained from

$$\partial_s \mathbf{q}_i^*(s) = \mathbf{v}_i^*(s), \quad \partial_s \mathbf{v}_i^*(s) = \frac{1}{2} \zeta^* \mathbf{v}_i^*(s) + L^* \mathbf{v}_i^*(s), \quad (5)$$

where L^* is the dimensionless Liouville operator, and $\zeta^* = \mathcal{L}^* \zeta(t)/v(t)$ is the dimensionless cooling rate. This is the same as the usual dynamics for hard spheres, except that the term proportional to $\zeta^*/2$ represents an acceleration between collisions which balances the energy lost during collisions, thus enabling a steady state.

Although it is possible to relate average values of the relevant dynamical functions of the original variables with the average values of the same functions of the scaled variables for a general situation, attention will be restricted in the following to the HCS for which ζ^* is time independent. In principle, the scaled dynamics defined by Eq. (5) can be simulated for the properties of interest, without the complications of continuous cooling in real time. In this formulation, the simulation is qualitatively similar to that for elastic collisions, in the sense that the system rapidly approaches a state for which the time average of the instantaneous scaled temperature is constant, and subsequent determination of average properties is simpler and numerically more accurate. A technical complication is the need to know the exact value of ζ^* *a priori*, which in general is not possible, since it is determined by the original dynamics. Consequently, it is useful to make a second change of scale,

$$\begin{aligned} \mathbf{q}_i^{**} &= \mathbf{q}_i^*, & \mathbf{v}_i^{**} &= (w^*/\zeta^*) \mathbf{v}_i^*, \\ s^* &= (\zeta^*/w^*) s, & A^{**}(s^*) &= A(s), \end{aligned} \quad (6)$$

where w^* is an arbitrary time-independent dimensionless frequency. Equation (5) then becomes

$$\begin{aligned} \partial_{s^*} \mathbf{q}_i^{**}(s^*) &= \mathbf{v}_i^{**}(s^*), \\ \partial_{s^*} \mathbf{v}_i^{**}(s^*) &= \frac{1}{2} w^* \mathbf{v}_i^{**}(s^*) + L^{**} \mathbf{v}_i^{**}(s^*), \end{aligned} \quad (7)$$

with L^{**} the same L^* , but with the replacements $\{\mathbf{q}_i^*, \mathbf{v}_i^*\} \rightarrow \{\mathbf{q}_i^{**}, \mathbf{v}_i^{**}\}$. This is the form most convenient for MD simulation, with any reasonable choice for w^* . More explicitly, the particle dynamics implied by Eq. (7) and implemented in our event-driven simulations consists of an accelerating streaming between collisions

$$\begin{aligned} \partial_{s^*} \mathbf{q}_i^{**} &= \mathbf{v}_i^{**}, \\ \partial_{s^*} \mathbf{v}_i^{**} &= \frac{1}{2} w^* \mathbf{v}_i^{**}, \end{aligned} \quad (8)$$

while the effect of the collision of two particles is to alter their relative velocity according to

$$\mathbf{g}_{ij}^{**} \rightarrow \tilde{\mathbf{g}}_{ij}^{**} = \mathbf{g}_{ij}^{**} - (1 + \alpha)(\hat{\mathbf{q}}_{ij}^{**} \cdot \mathbf{g}_{ij}^{**}) \hat{\mathbf{q}}_{ij}^{**}, \quad (9)$$

where $\mathbf{g}_{ij}^{**} = \mathbf{v}_i^{**} - \mathbf{v}_j^{**}$, $\hat{\mathbf{q}}_{ij}^{**}$ is the unit vector pointing from atom i to atom j and the center of mass velocity remains the same.

The relationship of ζ^* to w^* is determined by the steady-state temperature obtained in the simulation. To see this note that while the instantaneous kinetic energy of the entire system is clearly not constant, a corresponding ‘‘temperature’’ defined as $T^{**} = d^{-1} \langle v_1^{**2}; s^* \rangle^{**}$ does approach a constant, as is shown in Appendix A,

$$\begin{aligned} T^{**}(s^*) &= \frac{1}{2} \left(\frac{w^*}{\zeta^*} \right)^2 \left\{ 1 + \left[\frac{w^*}{\zeta^* \sqrt{2T^{**}(0)}} - 1 \right] e^{-w^* s^*/2} \right\}^{-2} \\ &\rightarrow \frac{1}{2} \left(\frac{w^*}{\zeta^*} \right)^2. \end{aligned} \quad (10)$$

Thus, $\zeta^* = w^*/\sqrt{2T^{**}(\infty)}$ which relates quantities measured during the steady-state simulation to those calculated in [1]. In summary, simulation of Eqs. (7) is expected to yield a steady state after a short transient period. Subsequently, ensemble averages of properties can be determined as time averages by making the usual assumption of ergodicity. These properties are directly related to those of the HCS by a simple scale transformation as described above.

This steady-state simulation method removes any limitation on the time for which trajectories may be followed, but there are other limitations due to a long wavelength hydrodynamic instability [3] for systems with dimension larger than a critical size $L_c = 2\pi\ell/\sqrt{2\eta^*/\zeta^*}$ where $\eta^* = \eta(t)/nmv(t)\ell$ is the shear viscosity. These instabilities occur when the decay rate of a shear mode fluctuation is less than the cooling rate of the thermal velocity so that their size grows relative to the temperature. In the scaled dynamics, the instabilities show up as ordinary unstable modes that grow exponentially with s^* , and are therefore easily identified in the simulations [5]. Since these growing modes represent a spontaneous breaking of the (assumed) spatial homogeneity of the system, the impurity particle no longer undergoes simple diffusion and, therefore, its motion is beyond the scope of this paper. The critical size L_c is a function of the density and coefficient of restitution, being smaller for high density and small restitution coefficient. In all the cases reported here, the system size is smaller than that required for the instability to show up. For a system of 108 atoms and $n^* \leq 0.5$, this provides no limitation on the accessible densities and coefficients of restitution, otherwise only sufficiently low (high) values of the density (coefficient of restitution) can be studied. A different limitation on the simulation is the ‘‘inelastic collapse’’ [6], which occurs for small values of α thereby setting a lower limit on the values accessible to simulation. For the system sizes considered in this paper, the above-mentioned limits have been characterized in more detail elsewhere [5].

The three-dimensional simulations reported in the following begin in all cases with an equilibrated fluid subject to elastic collisions (i.e., $\alpha = 1, w^* = 0$) with $T^{**} = 1/2$. The co-

efficient of restitution is then set to the desired value and the scaling parameter w^* is set to $w^* = \zeta_E^*(\alpha) \sqrt{2T^{**}(0)}$ using the Enskog estimate for the cooling rate $\zeta_E^*(\alpha)$ as given by Eq. (74) in Ref. [1]. This choice ensures that the temperature remains of order 1 for all values of α , for optimal numerical stability, as well as provides a continuous path to the equilibrium system for which $\alpha=1$ and $w^*=0$. The simulation is then continued for 10^7 collisions to allow the system to reach the steady state at $T^{**} = w^{*2}/2\zeta^{*2}$ where ζ^* is the true cooling rate generated by the simulation. Since the largest system considered consists of 500 atoms, this corresponds to at least 2×10^4 collisions per atom, and is more than sufficient to reach the steady state. A final simulation of 10^7 additional collisions is then performed, during which all statistical averages of interest are accumulated. Figure 1 shows the behavior of the instantaneous kinetic energy (or temperature) during several typical simulations. In all cases, the instantaneous temperature fluctuates around a stationary average value, with the size of the fluctuations increasing as the coefficient of restitution decreases. The fact that the average value itself varies with α is due to (a) the inadequacy of our knowledge of ζ^* for small values of α and (b) to the presence of long-lived shear fluctuations, or vortices, which decay on a time scale of thousands of collisions near the instability. As will be discussed below, the latter give rise to large fluctuations in all components of the kinetic contribution to the pressure tensor as well as raising the apparent temperature.

The system is expected to show a typical diffusive behavior under the scaled dynamics after a short transient time, i.e., for $s^* \gg 1$. Then the diffusion coefficient can be obtained either from the mean-squared displacement (MSD) using the Einstein relation, Eq. (70) of Ref. [1], or from the Green-Kubo relation, Eq. (69) of Ref. [1]. The former is evaluated, for $d=3$, from

$$\begin{aligned} D^{**}(s^*) &= \frac{w^*}{\zeta^*} D^*(s) \\ &= \frac{1}{6(N+1)} \frac{\partial}{\partial s^*} \sum_{i=0}^N |\mathbf{q}_i^{**}(s^*) - \mathbf{q}_i^{**}(0)|^2 \end{aligned} \quad (11)$$

by a least-squares fit of the simulation data to a straight line. We find little difference in the final value obtained using a single fit of the entire data set and the average of multiple fits performed on subsets of the data. The reported results are based on the former method. Figure 2 shows some typical simulation data exhibiting the expected linearity of the mean-square displacement as a function of s^* . The Green-Kubo relation for identical particles expresses the diffusion coefficient in terms of the velocity autocorrelation function (VACF) as

$$D^{**}(s^*) = \frac{1}{3} \int_0^{s^*} ds' \langle \mathbf{v}^{**}(s') \cdot \mathbf{v}^{**} \rangle^{**}. \quad (12)$$

The VACF is evaluated from

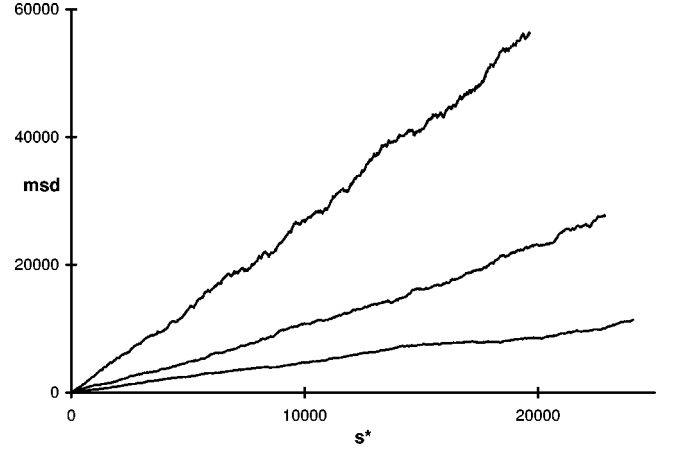


FIG. 2. Average mean-square dimensionless displacement (MSD) as a function of the dimensionless time in the steady-state dynamics for $n^*=0.5$. The lower curve is for $\alpha=1$, the middle for $\alpha=0.7$, and the upper for $\alpha=0.5$.

$$\begin{aligned} \langle v_{\alpha}^{**}(s^*) v_{\beta}^{**}(0) \rangle &= \frac{1}{(N+1)(j_{\max}+1)} \\ &\times \sum_{i=0}^N \sum_{j=0}^{j_{\max}} v_{i\alpha}^{**}(s^* + j\Delta^{**}) \\ &\times v_{i\beta}^{**}(j\Delta^{**}), \end{aligned} \quad (13)$$

where $\alpha, \beta = x, y, z$, Δ^{**} is the sampling period, and j_{\max} is a function of the amount of data available and the time at which the steady state is established. Notice that the stationarity of the scaled dynamics is explicitly used to evaluate the VACF for a given time separation s^* , by averaging over many different samplings during the simulation. In the simulations, Δ^{**} is taken to be 1/4 of the Boltzmann mean free time at $T^{**} = 1/2$, i.e., $\Delta^{**} = \sqrt{2}/16\sqrt{\pi}$. As discussed above, $T^{**} = 1/2$ is not the exact value of the converged temperature, but in formulating Δ^{**} only a reasonable order of magnitude is required. To evaluate the right side of Eq. (13), we follow the procedure of Futrelle and McGinty [7] (see also the discussion in Ref. [9]), according to which the components of the velocity for each atom sampled at intervals of Δ^{**} are stored. When the number of values stored reaches a threshold N_{Δ} , the convolution theorem is used to evaluate Eq. (13) by means of the fast Fourier transform, and so to obtain an estimate of the velocity autocorrelation function. This procedure is then repeated until the end of the simulation and the various estimates, typically between tens and hundreds of samples, are averaged to obtain the final estimate of the correlation function. Figure 3 shows some typical correlation functions obtained in this way, using $N_{\Delta} = 1024$. Here and below, we concentrate on the function C_{vv}^* , as defined in the preceding paper which is just the trace of Eq. (13) divided by its initial value. To get the diffusion constant, the integral of the velocity correlation function is computed using Simpson's rule and the variance of the pool of estimates is used as the basis for the calculation of the standard error.

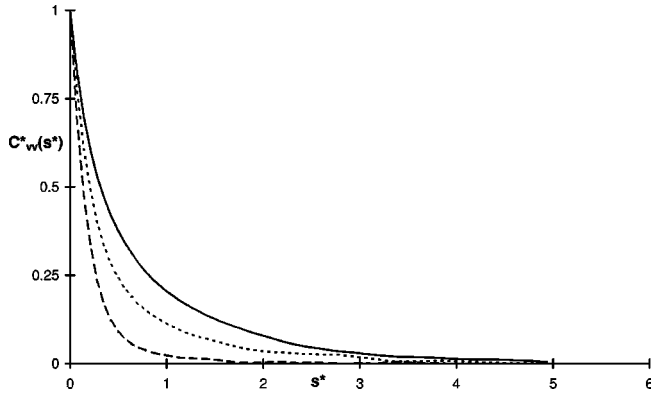


FIG. 3. Normalized velocity autocorrelation function $C_{vv}^*(s^*)$ as a function of the dimensionless scaled time s^* in the steady-state dynamics for $n^*=0.5$. The values of the coefficient of restitution are $\alpha=1$ (lower curve), $\alpha=0.7$ (middle curve), and $\alpha=0.5$ (upper curve).

Both methods, the Einstein relation and Green-Kubo relation, should yield the same values of the coefficient of self diffusion. Figures 2 and 3 show that the mean-square displacement becomes linear in s^* and the velocity autocorrelation function decays to zero for $s^* \geq 10$. For larger s^* both forms for the diffusion coefficient approach a constant, and all further discussion is restricted to this *diffusion constant*. The consistency between the Green-Kubo and Einstein relations is confirmed in Fig. 4, where the estimates obtained by both procedures are compared for a system of 108 atoms and several values of the density and of the coefficient of restitution. While in qualitative agreement, the difference in values obtained by the two methods is in some cases as great as 10%. It is expected that the results based on the velocity autocorrelation function are more accurate, because the evaluation at each fixed time s^* , is based on an average over all times included in the simulation. In contrast, the mean-square displacement is obtained from a single evaluation for each s^* . This qualitative difference in accuracy has been

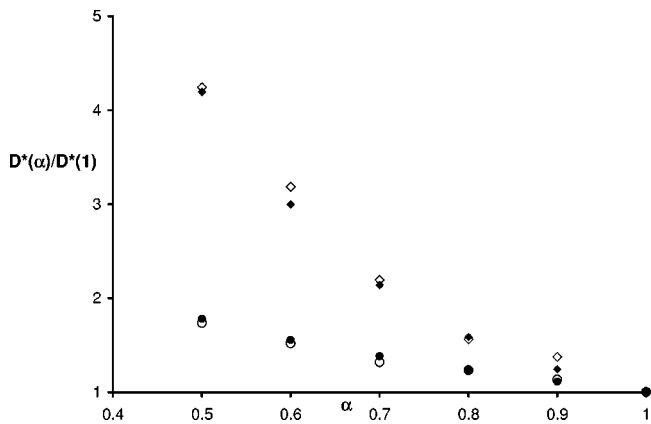


FIG. 4. Diffusion constant as a function of α for $n^*=0.1$ (circles) and $n^*=0.5$ (diamonds), as determined from the mean-squared displacement (open symbols) and the velocity autocorrelation function (full symbols). The values are normalized with those obtained for $\alpha=1$.

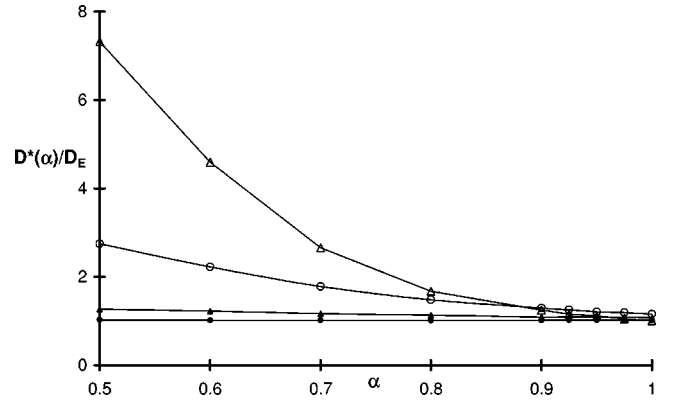


FIG. 5. Ratio of the diffusion constant determined by MD to the predicted value based on the Enskog theory, as a function of α , for $n^*=0.1$ (full circles), $n^*=0.25$ (full triangles), $n^*=0.5$ (open circles), and $n^*=0.75$ (open triangles). The lines are a guide to the eye.

confirmed by running multiple simulations for a few systems, and observing variations in the coefficient of self diffusion as large as 10% when determined from the MSD, whereas that determined from the VACF showed variations of less than 1%.

III. COMPARISON BETWEEN MD AND THEORY

Figure 5 shows the ratio of the observed diffusion constants to the value predicted by the Enskog-level theory, as a function of α for densities $n^*=0.1, 0.25, 0.5$, and 0.75 . For the lowest density, theory, and simulation are in excellent agreement even at strong dissipation, as expected from earlier comparisons of simulation results and predictions of the Boltzmann-Enskog equation [2]. As the density increases, deviations from the Enskog prediction are expected, since they are known to occur even at equilibrium ($\alpha=1$). In this respect, our results for $\alpha=1$ are quite consistent with previous studies of elastic hard spheres [8]. It is seen in the figure that deviations increase with decreasing α . For example, at $n^*=0.25$ the deviations are less than 10% for $\alpha \geq 0.9$, but increase rapidly to the order of 25% for $\alpha=0.5$. This behavior can also be observed in the normalized VACF itself which, in the Enskog approximation (here and below we refer to the first Sonine approximation to the Enskog theory), is given by $\exp(-\omega_1^{**} s^*)$, with [1]

$$\omega_1^{**} = \frac{2(1+\alpha)^2}{3} \chi(\pi T^{**})^{1/2}, \quad (14)$$

where χ is the pair-correlation function for two particles in contact for which we use the Carnahan-Starling estimate. Combined with Eq. (12) this corresponds to $D_E^{**}(\alpha) = \sqrt{2} T^{**} \omega_1^{** -1}$. In Fig. 6, the logarithm of the normalized velocity autocorrelation function, $C_{vv}^{**}(s^*)$, is plotted as a function of $\omega_1^{**} s^*$, for the case of *elastic* collisions, $\alpha=1$, and the several densities we have been considering. Here and below the choice has been made, somewhat arbitrarily but consistently, of truncating the VACF at $\ln C_{vv}^{**}(s^*) \simeq -4$ in

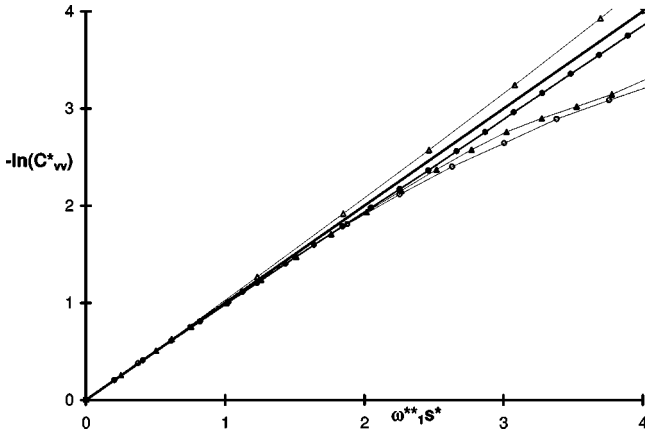


FIG. 6. Negative logarithm of the normalized VACF C_{vv}^* as a function of time for a system in equilibrium ($\alpha=1$). Symbols are as in Fig. 5. The lines are a guide to the eye, except the full line, which indicates the Enskog result.

order to eliminate the tails which are dominated by noise. The data confirm findings of earlier studies [8] that the Enskog theory gives a good description at low densities, but increasingly underestimates the diffusion constant, due to the neglect of correlated collisions and cage effects, at higher densities with a maximum deviation around $n^*=0.5$. Above this density, the neglected processes begin to cancel one another and near $n^*=0.75$, the diffusion constant crosses the Enskog prediction, and for higher densities is overestimated by Enskog theory. Since the Enskog theory is exact at short times [1], these effects appear as deviations from the simple exponential form of the VACF at longer times.

Now consider $\alpha < 1$. A similar plot, Fig. 7, for an inelastic system with $\alpha=0.7$, again shows good agreement with the Enskog prediction at the lowest density, but it exhibits much larger deviations than in the elastic case at higher densities, except at short times where the Enskog theory is exact, as already pointed out. Interestingly, the data clearly indicate a crossover to a slower constant decay rate at longer times. Of

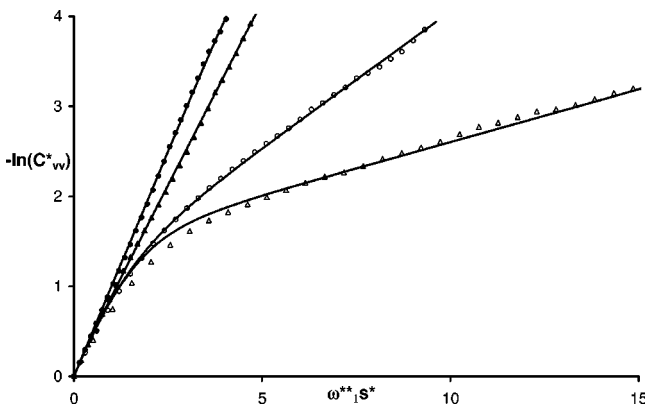


FIG. 7. Negative logarithm of the normalized VACF C_{vv}^* as a function of dimensionless time for the steady-state dynamics with $\alpha=0.7$. Symbols are as in Fig. 5. The lines are the results of fits of the memory function model with an exponential kernel as discussed in the main text. The lowest-density results are indistinguishable from the Enskog prediction on this scale.

course, this behavior increases the time integral of the velocity autocorrelation function, and it is responsible for the enhancement of the diffusion coefficient seen in Fig. 5, in contrast to the opposite behavior for high densities at $\alpha=1$.

To characterize the deviation of the VACF from the simple exponential form, we start with an exact expression for the VACF based on the Zwanzig-Mori formalism (see Appendix B),

$$\begin{aligned} \partial_{s^*} C_{vv}^{**}(s^*) + \omega_1^{**} C_{vv}^{**}(s^*) \\ + \int_0^{s^*} ds' M(s^* - s') C_{vv}^{**}(s') = 0, \end{aligned} \quad (15)$$

where $M(s^*)$ is known as the memory function. If $M(s^*)$ is neglected, the exponential decay of the above Enskog approximation is recovered, so the memory function incorporates all of the effects neglected in that approximation. A simple ansatz for this function as an exponential is qualitatively successful in modeling the VACF of fluids with elastic collisions (see [8] and references therein), and can be expected to work also for inelastic systems, when formulated in the dimensionless time s^* . If we substitute $M(s^*) = M(0)\exp(-\lambda s^*)$ into Eq. (15), and solve for the VACF with the boundary condition $C_{vv}^{**}(0) = 1$, the resulting model is

$$\begin{aligned} C^{**}(s^*) = \frac{\gamma_- - 1}{\gamma_- - \gamma_+} \exp(-\gamma_+ \omega_1^{**} s^*) \\ + \frac{\gamma_+ - 1}{\gamma_+ - \gamma_-} \exp(-\gamma_- \omega_1^{**} s^*), \end{aligned} \quad (16)$$

where the constants γ_+ and γ_- can be related to $M(0)$ and λ . Figure 7 includes the result of fitting these two parameters to the data, being evident that the above model is able to capture the crossover from the Enskog behavior at short times to the slower relaxation for longer times.

While the memory function model provides a framework for describing the results of the simulations, it does not explain them, since any effect not captured in the Enskog theory will give rise to a nonzero contribution to the memory function. In a previous study [5], similar deviations from the Enskog theory were found for the pressure of the system, and evidence was provided there suggesting that the large discrepancies between theory and simulation for dense, dissipative states may be due to the underlying hydrodynamic instability. Additional support for this possibility comes from Fig. 8 which shows the diffusion constants obtained from the simulation data for systems composed by 500 particles compared to those for systems composed by only 108 particles. For a density of $n^*=0.25$, there is a significant further increase of the diffusion constant in the large system relative to the small system as α decreases, with the diffusion constant of the 500 atom system growing to almost twice that of the 108 atom system at $\alpha=0.5$. At $n^*=0.5$, the enhancement is even larger, but we know [5] that the system is in the unstable regime, at least for $\alpha \leq 0.7$ and possibly for smaller values, so that most of the enhancement is undoubtedly due

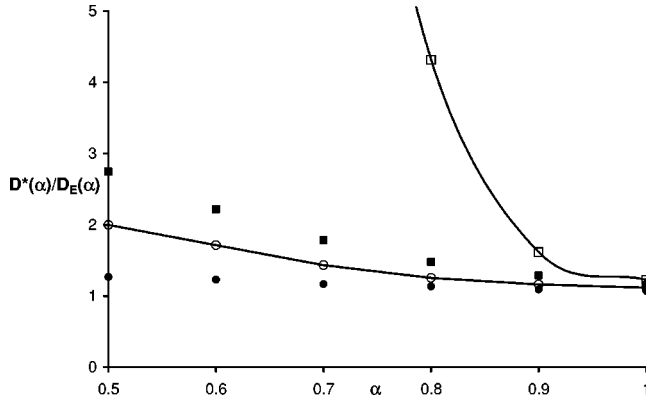


FIG. 8. Diffusion constants for $n^*=0.25$ (circles) and $n^*=0.50$ (squares) as a function of α , for 108 atoms (full symbols) and 500 atoms (open symbols). The values are normalized to the α -dependent Enskog prediction. The lines are a guide to the eye.

to the spontaneous formation of shear flow in the system. This suggests that in the smaller systems, although they are stable, there are present large fluctuations characteristic of the instability, such as spontaneous vortices that form and breakup. In this case, the impurity would find itself in a fluctuating local flow field which could enhance the velocity correlations.

To test whether a local flow field plays a relevant role in the self-diffusion process, two different methods were used to calculate the autocorrelation of the impurity velocity *relative to the instantaneous local flow field*. In the first method, the instantaneous local flow field was calculated by dividing the simulation cell into $3^3=27$ cubic subcells. Then each atom's velocity relative to the instantaneous average velocity of the fluid in the subcell containing it, was used when calculating both the temperature and the VACF. For the 108 particle system, this procedure leads to a lowering of the measured value of the equilibrium diffusion constant by

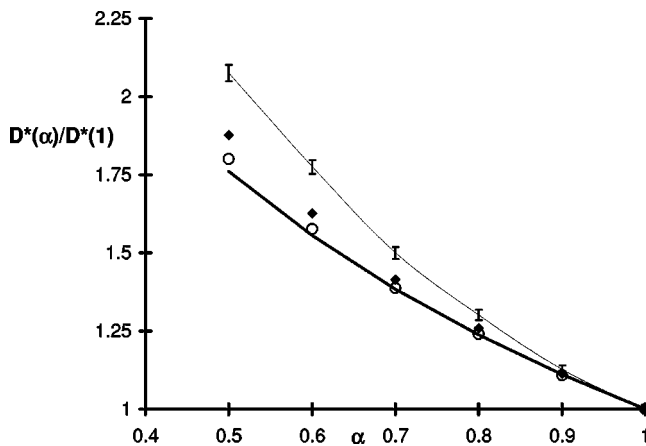


FIG. 9. Diffusion constants for $n^*=0.25$ as a function of α for 108 atoms, calculated from the Green-Kubo relation (error bars and connecting line), by removing the longest Fourier modes (diamonds), and by using the cell method of computing the local velocity field (circles). All data are normalized to the values determined for $\alpha=1$. The heavy line is the prediction from Enskog theory.

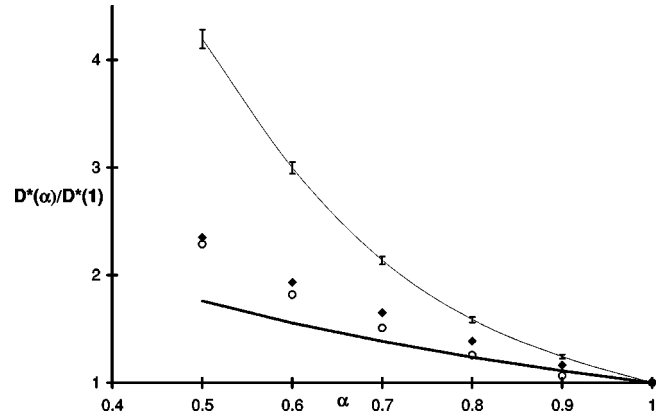


FIG. 10. The same as Fig. 9 for $n^*=0.50$.

about 10%, which we believe to be a finite-size effect due to the removal of a significant fraction of the degrees of freedom of the system. For $n^*=0.5$ it also reduces the steady-state temperature from nearly twice the initial temperature (see Fig. 1) to about $1.5T^{**}(0)$ thus demonstrating the size of the contribution of these fluctuations to the temperature. When the same procedure is applied to a system of 500 atoms, the shift in the equilibrium diffusion constant is negligible. The results obtained by this method are presented in Figs. 9–11. In the graphs, the α -dependent diffusion constant has been scaled by its measured equilibrium value. The conclusion emerging from the figures is that the α dependence of the diffusion constant is substantially closer to the Enskog form. However, this method may be criticized on the grounds that the statistics of the local velocity field are poor, since the calculations only involve a few atoms in each cell. We, therefore, also consider a second method which is specifically designed to eliminate only the part of the local flow due to the longest wavelength fluctuations in the system. A local flow field \mathbf{u} is defined by summing over the smallest Fourier components compatible with the size and shape of the simulation cell,

$$u_\alpha(\mathbf{r}) = \sum_{|\mathbf{k}| \geq 2\pi/L} u_\alpha(\mathbf{k}) e^{i\mathbf{k}\cdot\mathbf{r}}, \quad (17)$$

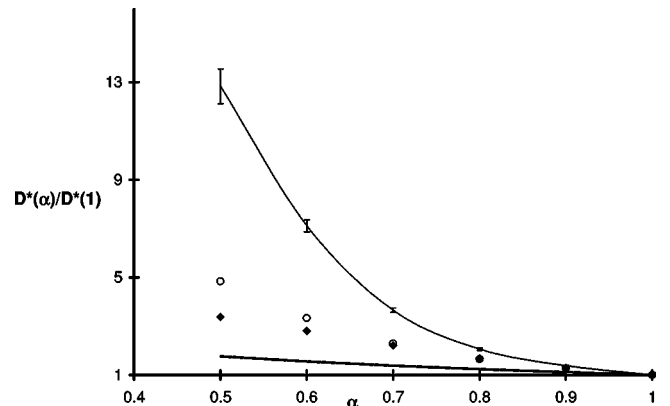


FIG. 11. The same as Fig. 9 for $n^*=0.75$.

where L^3 is the volume of the cubic simulation cell. The Fourier components are determined from the instantaneous velocities of the bulk fluid via

$$u_\alpha(\mathbf{k}) = \frac{2}{N+1} \sum_i v_{i\alpha} e^{-i\mathbf{k}\cdot\mathbf{r}_i}. \quad (18)$$

This method is expected to give better statistics than the cell method discussed above. We then use this flow field to define the relative velocity used in the calculation of the temperature and the VACF. Figures 9–11 also show the resulting diffusion constant when this method of subtracting the instantaneous fluctuations is used. From the figures follows that both methods are mutually consistent over the range $0.5 < \alpha < 1$, and that the agreement between the simulation results and the theoretical prediction from Enskog theory is significantly improved. The effects of subtracting the local flow field are much larger for the inelastic case due to the mechanism responsible for shear instability.

IV. DISCUSSION

In this paper, we have continued the discussion of diffusion in a model granular system begun in Ref. [1]. The main motivation has been to show that transformation to the steady-state dynamics allows us to carry over many standard methods of nonequilibrium statistical mechanics with relatively minor modifications. Here, the exact correspondence between the usual formulation of the dissipative hard-sphere model of granular fluids and the steady-state dynamics was exploited to formulate a particularly convenient simulation method which eliminates the need for additional complications such as exothermic boundary conditions. We have demonstrated that in the steady-state variables, the homogeneous cooling state exhibits standard diffusive behavior such as the linear increase of the mean-squared displacement with time, and the correspondence between the Einstein and Green-Kubo methods of determining the diffusion constant. In addition, the simplest approximation of Enskog kinetic theory provides excellent agreement at low densities for the whole range of inelasticity $0.5 \leq \alpha \leq 1$. However, although the formalism and concepts of the statistical mechanics of diffusion have been shown to give an adequate description of diffusion in the HCS, large quantitative deviations from the Enskog kinetic theory predictions have been observed even at relatively moderate densities. At the level of the VACF, it was shown that the deviations are principally due to a crossover from the Enskog time dependence, which is exact for short times, to another, slower decay which nevertheless also appears to be exponential in form. The analytic form of the VACF was shown to be well approximated by modeling the memory function of the diffusive process by a simple exponential as has been used in early studies of memory effects in equilibrium fluids [8].

Physically, we have shown by means of constrained simulations that the deviations from the Enskog model are primarily due to the effect of the longest wavelength velocity modes in the system. For sufficiently large systems, the shear mode is linearly unstable (in the steady-state picture) in the

classic sense that the time constant associated with its decay goes to zero as the critical value of α is approached from above. A linear stability analysis in the steady-state variables [5] shows that the shear fluctuations of wave-vector k decay exponentially with a time constant of $\eta^* k^{*2} - \frac{1}{2} \zeta^*$, where η^* is the shear viscosity and the stars indicate quantities expressed in the reduced units of [1]. The dominant α dependence of this expression comes from $\zeta^* \sim (1 - \alpha^2)$ and the size of the system enters through the fact that the smallest nonzero value of the wave vector the system can sample is $k_{\min}^* = 2\pi/L^*$, where L^* is the longest dimension of the simulation cell. For fixed values of $\alpha < 1$, there will always be a critical value of L^* above which the system is unstable to shear fluctuations. For values of α above the critical value, the decay of these fluctuations is nevertheless slowed relative to equilibrium and we therefore reason that, even before the onset of the instability and even in systems too small to exhibit the instability, the slowing down of this mode means that long-lived, long-wavelength fluctuations are present. These fluctuations give rise to the observed enhancement of the diffusion constant. This effect is somewhat analogous to what is observed in turbulent systems since the removal of these modes in the calculation of the diffusion constant removed a large part of the discrepancy from the Enskog prediction. The size dependence of the deviations from the Enskog results supports this conclusion, since larger systems have a higher critical value of α because the wave vector can take on smaller values. We conclude that a complete theoretical description of diffusion in HCS will require a model for the memory function taking into account the slow relaxation of the shear modes by means, e.g., of a mode-coupling mechanism.

ACKNOWLEDGMENTS

The research of J.W.D. was supported by the National Science Foundation, Grant No. PHY 9722133. J.J.B. acknowledges partial support from the Dirección General de Investigación Científica y Técnica (Spain) through Grant No. PB98-1124. J.L. acknowledges support from the Université Libre de Bruxelles.

APPENDIX A: APPROACH TO STATIONARITY

The average value of an observable $A(\Gamma)$ for a general homogeneous state $\rho(\Gamma, t)$ is given by Eq. (4) above which can be written

$$\langle A; t \rangle = \int d\Gamma^* \rho^*(\Gamma^*) A(\{\mathcal{L} \mathbf{q}_i^*(s), v(t) \mathbf{v}_i^*(s)\}) \quad (A1)$$

and

$$\partial_s \mathbf{q}_i^*(s) = \mathbf{v}_i^*(s), \quad \partial_s \mathbf{v}_i^*(s) = \frac{1}{2} \zeta_{\text{HCS}}^* \mathbf{v}_i^*(s) + L^* \mathbf{v}_i^*(s). \quad (A2)$$

The subscript on ζ_{HCS}^* indicates explicitly that it is the dimensionless cooling rate associated with the HCS

$$\zeta_{\text{HCS}}^* = \frac{\ell \zeta_{\text{HCS}}(t)}{v_{\text{HCS}}(t)}, \quad (\text{A3})$$

where ℓ is the mean free path and $v_{\text{HCS}}(t) = \sqrt{2T_{\text{HCS}}(t)/m}$ is the HCS thermal velocity. The temperature $T_{\text{HCS}}(t)$ obeys the equation

$$\partial_t T_{\text{HCS}}(t) = -\zeta_{\text{HCS}}[T_{\text{HCS}}(t)]T_{\text{HCS}}(t). \quad (\text{A4})$$

Now make the change of variables

$$\begin{aligned} \mathbf{q}_i^{**} &= \mathbf{q}_i^*, & \mathbf{v}_i^{**} &= (w^*/\zeta_{\text{HCS}}^*)\mathbf{v}_i^*, \\ s^* &= (\zeta_{\text{HCS}}^*/w^*)s, & A^{**}(s^*) &= A(s), \end{aligned} \quad (\text{A5})$$

to get

$$\begin{aligned} \langle A; t \rangle &= \int d\Gamma^{**} \rho^{**}(\Gamma^{**}, s^*) A(\{\ell \mathbf{q}_i^{**}, v(t) \\ &\quad \times (\zeta_{\text{HCS}}^*/w^*)\mathbf{v}_i^{**}\}), \end{aligned} \quad (\text{A6})$$

with the definition $d\Gamma^{**} \rho^{**}(\Gamma^{**}, s^*) \equiv d\Gamma^* \rho^*(\Gamma^*, s)$. In particular, the kinetic energy is

$$\begin{aligned} \left\langle \frac{1}{2} m v^2; t \right\rangle &= v_{\text{HCS}}^2(t) (\zeta_{\text{HCS}}^*/w^*)^2 \\ &\quad \times \int d\Gamma^* \rho^*(\Gamma^*, s) \frac{1}{2} m v^{**2} \\ &\equiv \frac{1}{2} m v_{\text{HCS}}^2(t) (\zeta_{\text{HCS}}^*/w^*)^2 \langle v^{**2}; s^* \rangle^{**}. \end{aligned} \quad (\text{A7})$$

The corresponding temperature is

$$T(t) = \frac{2}{d} \left\langle \frac{1}{2} m v^2; t \right\rangle = 2 T_{\text{HCS}}(t) \left(\frac{\zeta_{\text{HCS}}^*}{w^*} \right)^2 T^{**}(s^*), \quad (\text{A8})$$

where $T^{**}(s^*) \equiv d^{-1} \langle v^{**2}; s^* \rangle^{**}$. The time derivative of $T^{**}(s^*)$ is then found to be

$$(\partial_{s^*} - w^*) T^{**}(s^*) = -w^* \frac{\zeta(t)}{\zeta_{\text{HCS}}(t)} T^{**}(s^*). \quad (\text{A9})$$

This is still valid for a general homogeneous state. Now assume the existence of a scaling solution, which implies $\zeta(t)/\zeta_{\text{HCS}}(t) = \sqrt{T(t)/T_{\text{HCS}}(t)}$. Then

$$(\partial_{s^*} - w^*) T^{**}(s^*) = -\sqrt{2} \zeta_{\text{HCS}}^* T^{**3/2}(s^*). \quad (\text{A10})$$

The solution is that given by Eq. (10) of the text.

APPENDIX B: MEMORY FUNCTION MODEL

The dimensionless velocity auto correlation function is defined by

$$C_{vv}^*(s) \equiv \langle \psi(s) \psi \rangle^*, \quad \psi = \frac{v_{0x}^*}{\sqrt{\langle v_{0x}^{*2} \rangle^*}}. \quad (\text{B1})$$

Using the notation in Ref. [1] this can be written in terms of the generators of the dynamics

$$C_{vv}^*(s) = \int d\Gamma^* (e^{\mathcal{L}^* s} \psi) \rho_{\text{HCS}}^* \psi = \int d\Gamma^* \psi e^{-\bar{\mathcal{L}}^* s} (\rho_{\text{HCS}}^* \psi). \quad (\text{B2})$$

The detailed forms for the linear operators \mathcal{L}^* and $\bar{\mathcal{L}}^*$ are given by Eqs. (36) and (42) of Ref. [1] but will not be required here. A projection operator is defined by

$$PX = \rho_{\text{HCS}}^* \psi \int d\Gamma^* \psi X. \quad (\text{B3})$$

It follows then that

$$PX(s) = \rho_{\text{HCS}}^* \psi C_{vv}^*(s), \quad (\text{B4})$$

with the choice

$$X(s) = e^{-\bar{\mathcal{L}}^* s} (\rho_{\text{HCS}}^* \psi). \quad (\text{B5})$$

The equation of motion for $X(s)$ is

$$(\partial_s + \bar{\mathcal{L}}^*) X(s) = 0 \quad (\text{B6})$$

and a closed equation for $PX(s)$ is obtained by operating on this equation with P and $Q = 1 - P$ to get the pair of equations

$$(\partial_s + P \bar{\mathcal{L}}^* P) PX(s) = -P \bar{\mathcal{L}}^* Q X(s),$$

$$(\partial_s + Q \bar{\mathcal{L}}^* Q) Q X(s) = -Q \bar{\mathcal{L}}^* P X(s). \quad (\text{B7})$$

Solving formally for $QX(s)$ in the second equation and substituting into the first gives the desired closed equation for $PX(s)$ [10],

$$\begin{aligned} (\partial_s + P \bar{\mathcal{L}}^* P) PX(s) - \int_0^s ds' e^{-Q \bar{\mathcal{L}}^* Q (s-s')} P \bar{\mathcal{L}}^* Q \bar{\mathcal{L}}^* P X(s') \\ = 0. \end{aligned} \quad (\text{B8})$$

Use of Eq. (B4) gives the corresponding equation for $C_{vv}^*(s)$,

$$\partial_s C_{vv}^*(s) + \omega_1 C_{vv}^*(s) + \int_0^s ds' M(s-s') C_{vv}^*(s') = 0, \quad (\text{B9})$$

with the definitions

$$\omega_1 = \int d\Gamma^* \psi \bar{\mathcal{L}}^* \rho_{\text{HCS}}^* \psi = \langle (\mathcal{L}^* \psi) \psi \rangle^* \quad (\text{B10})$$

and

$$M(s) = - \int d\Gamma^* \psi \bar{\mathcal{L}}^* e^{-Q\bar{\mathcal{L}}^* Qs} Q\bar{\mathcal{L}}^* \rho_{\text{HCS}}^* \psi. \quad (\text{B11})$$

The definition for ω_1 is the same as that for the Enskog

approximation discussed in [1] and approximated in Eq. (14) above. Finally, it is clear that structurally identical expressions would have been obtained had we performed this derivation using the scaled variables introduced in Eq. (6) of the text thus justifying the expression in Eq. (15).

-
- [1] J. W. Dufty, J. J. Brey, and J. Lutsko, Phys. Rev. E **65**, 051303 (2002).
 [2] J. J. Brey, M. J. Ruiz-Montero, D. Cubero, and R. García-Rojo, Phys. Fluids **12**, 876 (2000).
 [3] I. Goldhirsch and G. Zanetti, Phys. Rev. Lett. **70**, 1619 (1993).
 [4] R. Soto and M. Mareschal, Phys. Rev. E **63**, 041303 (2001); R. Soto, M. Mareschal, and M. M. Monsour, *ibid.* **62**, 3836 (2000).
 [5] J. F. Lutsko, Phys. Rev. E **63**, 061211 (2001).
 [6] S. McNamara and W. R. Young, Phys. Rev. E **53**, 5089 (1996).
 [7] R. P. Futrelle and D. J. McGinty, Chem. Phys. Lett. **12**, 285 (1971).
 [8] J. P. Boon and S. Yip, *Molecular Hydrodynamics* (McGraw-Hill, New York, 1980).
 [9] M. P. Allen and D. J. Tildesley, *Computer Simulation of Liquids* (Oxford University Press, Oxford, U.K., 1987).
 [10] B. Berne in *Statistical Mechanics—Part B*, edited by B. Berne (Plenum, New York, 1977).